Electronic and vibrational spectra of protonated benzaldehyde-water clusters, [BZ-(H2O)n≤5]H+: evidence for ground-state proton transfer to solvent for n ≥ 3.

Otto Dopfer, Alexander Patzer, Shamik Chakraborty, Ivan Alata, Reza Omidyan, Michel Broquier, Claude Dedonder, Christophe Jouvet

Electronic and vibrational spectra of protonated benzaldehyde-water clusters, [BZ-(H₂O)ₙ≤₅]H⁺: Evidence for ground-state proton transfer to solvent for n ≥ 3

Otto Dopfer,[1,a)] Alexander Patzer,[1] Shamik Chakraborty,[1] Ivan Alata,[2] Reza Omidyan,[2] Michel Broquier,[2] Claude Dedonder,[3] and Christophe Jouvet[3]

[1]*Institut für Optik und Atomare Physik, Technische Universität Berlin, Hardenbergstrasse 36, 10623 Berlin, Germany*
[2]*Institut des Sciences Moléculaires d'Orsay, UMR-CNRS 8214, and Centre Laser de l'Université Paris Sud/LUMAT FR 2764, Batiment 106, l'Université Paris Sud 11, 91405 Orsay Cedex, France*
[3]*Physique des Interactions Ioniques et Moléculaires, UMR-CNRS 7345 Aix Marseille Université, Avenue Escadrille Normandie-Niémen, 13397 Marseille Cedex 20, France*

Vibrational and electronic photodissociation spectra of mass-selected protonated benzaldehyde-(water)$_n$ clusters, [BZ-(H$_2$O)$_n$]H$^+$ with n ≤ 5, are analyzed by quantum chemical calculations to determine the protonation site in the ground electronic state (S$_0$) and $\pi\pi^*$ excited state (S$_1$) as a function of microhydration. IR spectra of [BZ-(H$_2$O)$_n$]H$^+$ with n ≤ 2 are consistent with BZH$^+$-(H$_2$O)$_n$ type structures, in which the excess proton is localized on benzaldehyde. IR spectra of clusters with n ≥ 3 are assigned to structures, in which the excess proton is located on the (H$_2$O)$_n$ solvent moiety, BZ-(H$_2$O)$_n$H$^+$. Quantum chemical calculations at the B3LYP, MP2, and ri-CC2 levels support the conclusion of proton transfer from BZH$^+$ to the solvent moiety in the S$_0$ state for hydration sizes larger than the critical value n$_c$ = 3. The vibronic spectrum of the S$_1$ ← S$_0$ transition ($\pi\pi^*$) of the n = 1 cluster is consistent with a cis-BZH$^+$-H$_2$O structure in both electronic states. The large blueshift of the S$_1$ origin by 2106 cm^{-1} upon hydration with a single H$_2$O ligand indicates that the proton affinity of BZ is substantially increased upon S$_1$ excitation, thus strongly destabilizing the hydrogen bond to the solvent. The adiabatic S$_1$ excitation energy and vibronic structure calculated at the ri-CC2/aug-cc-pVDZ level agrees well with the measured spectrum, supporting the notion of a cis-BZH$^+$-H$_2$O geometry. The doubly hydrated species, cis-BZH$^+$-(H$_2$O)$_2$, does not absorb in the spectral range of 23 000–27 400 cm^{-1}, because of the additional large blueshift of the $\pi\pi^*$ transition upon attachment of the second H$_2$O molecule. Calculations predict roughly linear and large incremental blueshifts for the $\pi\pi^*$ transition in [BZ-(H$_2$O)$_n$]H$^+$ as a function of n. In the size range n ≥ 3, the calculations predict a proton transfer from the (H$_2$O)$_n$H$^+$ solvent back to the BZ solute upon electronic $\pi\pi^*$ excitation. © *2014 AIP Publishing LLC.* [http://dx.doi.org/10.1063/1.4869341]

I. INTRODUCTION

In the past decade, the spectroscopic characterization of the structure, dynamics, vibrational, and electronic properties of isolated and microsolvated protonated and aromatic molecules (AH$^+$) has developed into an active research area. AH$^+$ ions occur as short-lived intermediates in chemical reaction mechanisms, combustion, hydrocarbon plasmas, and biochemical processes.[1] Moreover, protonated polycyclic aromatic hydrocarbon molecules and their derivatives are considered as possible carriers of the so-called unidentified infrared emission (UIR) and diffuse interstellar bands (DIB) observed in different interstellar media.[2–4]

Recent developments in the efficient generation of cold AH$^+$ ions in the gas phase and sensitive resonant vibrational and electronic photodissociation techniques enabled their spectroscopic characterization in the ground and elec-

tronically excited states. The major strategies for preparing cold AH$^+$ ions for spectroscopic interrogation are electrospray ionization (ESI) or chemical ionization in electron impact or discharge ion sources coupled with cryogenic ion traps or supersonic expansions.[3–11] Recently, IR and electronic spectra of cold AH$^+$ ions have been obtained in cryogenic H$_2$ and Ne matrices, respectively.[12]

Hydration of AH$^+$ has a profound impact on their structure and dynamics, as well as their chemical reactivity. Thus, microhydrated clusters of AH$^+$ are suitable model systems to study solute-solvent interactions and solvent-induced ion-molecule reactions at the molecular level,[13,14] including proton transfer, which is the most fundamental chemical reaction. [A-(H$_2$O)$_n$]H$^+$ clusters may exist in two different configurations, AH$^+$-(H$_2$O)$_n$ and A-(H$_2$O)H$^+$, which are connected by intracluster proton transfer. The preferred protonation site depends on the protonation affinities (PA) of the aromatic molecule and the solvent cluster, and the respective ion solvation energies. As the PA of (H$_2$O)$_n$ clusters increases substantially with cluster size n (Table I), often

a)Author to whom correspondence should be addressed. Electronic mail: dopfer@physik.tu-berlin.de. Fax: (+49) 30-31423018.

TABLE I. Proton affinities (PA) of benzaldehyde and $(H_2O)_n$ clusters (in kJ/mol).

Species	PA
H_2O	690 ± 4[a]
$(H_2O)_2$	808 ± 6[a], 824 ± 4[b]
$(H_2O)_3$	879 ± 4[b]
$(H_2O)_4$	913 ± 12[b]
BZ (S_0)	834[c]
BZ ($\pi\pi^*$)	970[d]

[a]Reference 41.
[b]Reference 16.
[c]Reference 42.
[d]Reference 10.

intracluster proton transfer from AH^+ to the water solvent network occurs above a critical cluster size, $n \geq n_c$.[8,14–18] Electronic excitation of AH^+ ions often has a drastic effect on the PA of A. As a consequence, excited state proton transfer to or from the solvent cluster may be triggered by electronic excitation depending on whether the PA of A decreases or increases upon electronic excitation. In addition to the energetics and chemical reactivity, also the dynamical relaxation processes of AH^+ may be strongly affected by solvation. For example, microhydration of protonated tryptophan increases the lifetime of the excited state from the femtosecond to the picoseconds timescale.[19] Finally, hydration may also change the preferred protonation site in AH^+. While such effects have not been detected for large protonated peptides with up to 50 H_2O molecules,[6] small bifunctional aromatic molecules may exhibit a switch in the protonation site from one to another functional group upon successive hydration.[20]

Here we use a combined mass spectrometric, spectroscopic, and quantum chemical approach to study the protonation site and solvent structure of microhydrated clusters of protonated benzaldehyde, $[BZ-(H_2O)_n]H^+$ in the size range $n \leq 5$. Benzaldehyde (BZ) is the simplest aromatic aldehyde and its protonation occurs preferentially at the carbonylic oxygen atom (oxonium).[7,11,21,22] Protonation at the aromatic ring (carbenium) is less favorable by >100 kJ/mol[11,22] and has not been observed yet. The oxonium ion of BZH^+ exists as planar cis and trans isomers with C_s symmetry (Fig. 1),
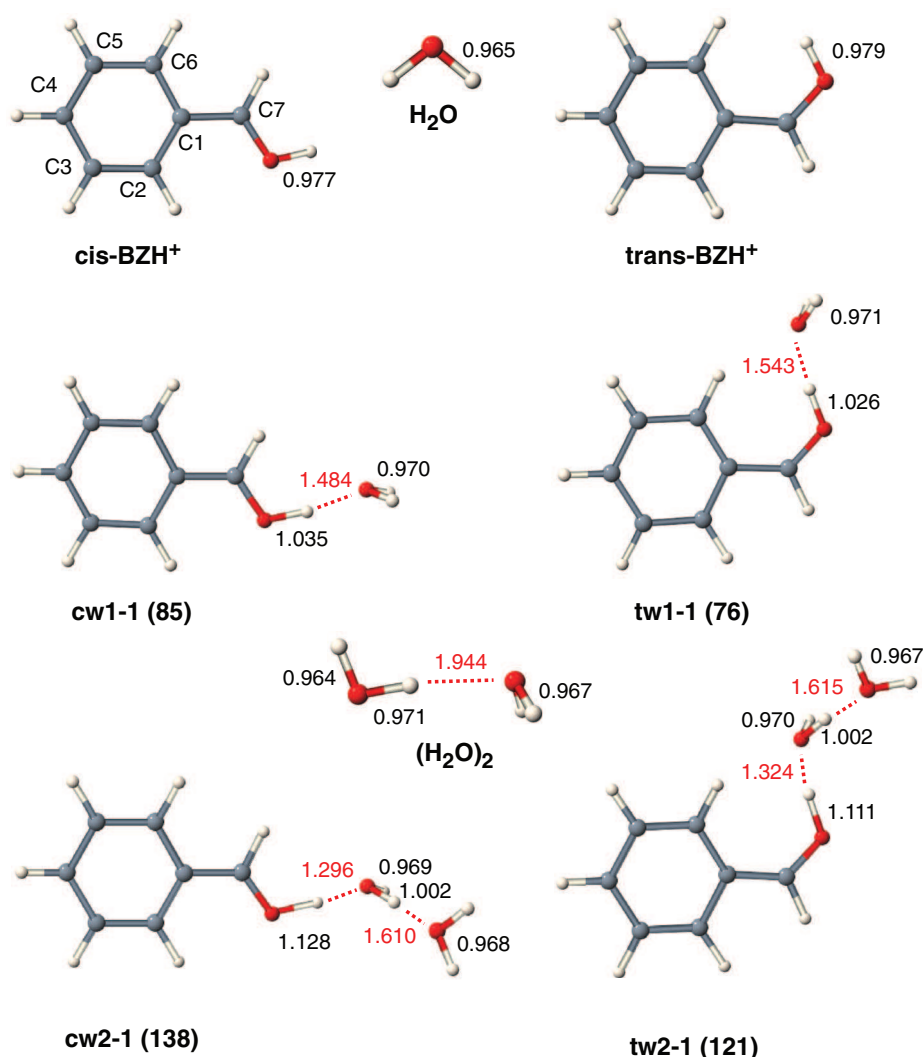

FIG. 1. Minimum energy structures of cis- and trans-BZH^+ and their most stable $[BZ-(H_2O)_n]H^+$ isomers ($n \leq 2$) calculated at the MP2/cc-pVDZ level. Structures for $(H_2O)_n$ with $n \leq 2$ are also given for reference. Bond lengths and total binding energies are given in Å and kJ/mol, respectively. trans-BZH^+ is less stable than cis-BZH^+ by 7 kJ/mol.

whereby cis-BZH$^+$ is calculated to be more stable than trans-BZH$^+$ by ~10 kJ/mol.[11,21,22] Both isomers were identified in superacids by NMR spectroscopy.[21] In the gas phase, oxonium ions of BZH$^+$ were first identified by early low-resolution UV photodissociation of mass-selected BZH$^+$ ions in an ion cyclotron resonance mass spectrometer (ICR-MS) at 300 K,[23] and their protonation site was further supported by mass spectrometry.[24] Initial spectral evidence for the preferential formation of cis-BZH$^+$ in the gas phase came from IR multiphoton dissociation in the fingerprint range measured in an ICR-MS at 300 K,[22] and vibrationally resolved electronic spectra of the $S_1 \leftarrow S_0$ transition ($\pi\pi^*$) of cold BZH$^+$ ions produced in a supersonic discharge expansion.[7] Definitive spectral identification of both cis-BZH$^+$ and trans-BZH$^+$ was obtained from IR photodissociation (IRPD) of BZH$^+$ and its weakly bonded BZH$^+$-L$_n$ clusters with L = Ar and N$_2$ produced in an electron impact supersonic plasma expansion.[11] It was found that, although the PA of cis-BZH$^+$ is slightly larger than for trans-BZH$^+$ (by ~10 kJ/mol), the H-bonds of ligands L to the acidic OH group of trans-BZH$^+$ are slightly less stable due to steric hindrance. Electronic spectra of the $S_1 \leftarrow S_0$ transition of cis-BZH$^+$-L with L = Ar and N$_2$ exhibit substantial blueshifts of the S_1 origin (300 and 628 cm^{-1}) from the corresponding monomer transition (23 470 cm^{-1}), indicating that the PA of BZH$^+$ increases substantially upon S_1 ($\pi\pi^*$) excitation leading to weaker intermolecular H-bonds to the ligands L in the excited state. Thus, the protonation site in the [BZ-(H$_2$O)$_n$]H$^+$ clusters studied here, depends not only on the hydration size (n) but also on the electronic state ($S_{0,1}$). It is noted that protonation of BZ changes the character of the S_1 state from $n\pi^*$ to $\pi\pi^*$.[7,10] Neglecting solvation energy effects, the PA values of BZ and (H$_2$O)$_n$ listed in Table I predict the excess proton in S_0 to be located on the BZ moiety for n ≤ 2 and on the solvent cluster for n ≥ 3, i.e. the expected critical hydration size for proton transfer to solvent in S_0 is n_c = 3. On the other hand, n_c will be larger in the S_1 state because of the increased PA of BZ. The large redshift in the $\pi\pi^*$ transition of cis-BZH$^+$ upon protonation (2.95 − 4.36 = −1.41 eV) implies that the PA of BZ increases drastically (by 136 kJ/mol) upon electronic excitation.[7,10] Thus, the PA values listed in Table I suggest that the excess proton in the $\pi\pi^*$ state of [BZ-(H$_2$O)$_n$]H$^+$ prefers to be attached to BZ at least up to n = 4 and most likely for much larger n. The current work addresses these issues experimentally and computationally by IR spectra of [BZ-(H$_2$O)$_n$]H$^+$ recorded in the O–H stretch range (n ≤ 5) and electronic spectra of the $S_1 \leftarrow S_0$ transition (n ≤ 2) in the vicinity of S_1 of BZH$^+$ (23 000–27 400 cm^{-1}), as well as quantum chemical calculations (n ≤ 4).

II. EXPERIMENTAL AND COMPUTATIONAL TECHNIQUES

A. IR spectroscopy

IR photodissociation (IRPD) spectra of [BZ-(H$_2$O)$_n$]H$^+$ clusters with n ≤ 5 are obtained in a tandem quadrupole mass spectrometer coupled to a supersonic electron impact plasma beam expansion and an octopole ion trap.[14,25]

[BZ-(H$_2$O)$_n$]H$^+$ are generated by electron and/or chemical ionization of the expanding gas mixture and subsequent ion-molecule and clustering reactions. The expanding gas mixture is obtained by passing 5% H$_2$ in He at a stagnation pressure of 2–5 bars through successive reservoirs filled with benzaldehyde and water kept at room temperature. The mass spectrum of this source (Fig. 2) reveals the presence of BZH$^+$ (m/z 107),[10] BZ$^+$ (m/z 106), the benzoyl cation (m/z 105),[26] and their water clusters. The BZH$^+$/BZ$^+$ abundance ratio of ~5 indicates efficient protonation under these experimental conditions. In general, the abundance of the [BZ-(H$_2$O)$_n$]H$^+$ clusters decreases rapidly with increasing n, indicating the sequential formation of the hydrated complexes. For example, the BZH$^+$/[BZ-(H$_2$O)$_n$]H$^+$ ratios in Fig. 2 are about 10 and 100 for n = 1 and 2, respectively. The desired [BZ-(H$_2$O)$_n$]H$^+$ ions are mass selected with the first quadrupole and irradiated in the adjacent octopole with tunable radiation from a pulsed IR-OPO laser pumped by a Q-switched ns Nd:YAG laser. The IR-OPO laser is characterized by pulse energies of 5–10 mJ in the 3000–4000 cm^{-1} range and a bandwidth of 1 cm^{-1}. The laser frequency has been calibrated by comparing atmospheric water absorptions along the IR laser path with the published spectrum.[27] All IRPD spectra are normalized for laser intensity variations measured with a pyroelectric detector. Resonant vibrational excitation of [BZ-(H$_2$O)$_n$]H$^+$ exclusively leads to the evaporation of one or two water ligands. The [BZ-(H$_2$O)$_m$]H$^+$ fragment ions generated by laser-induced dissociation (LID, denoted as n → m) are mass-selected using a second quadrupole and monitored as a function of the laser frequency to obtain the IRPD spectrum of the parent ions. As an example, Fig. 3 shows the mass spectra obtained by mass selecting [BZ-(H$_2$O)$_2$]H$^+$ (m/z 143) with the first quadrupole and scanning the second quadrupole without laser excitation (a), with resonant IR excitation at 3730 cm^{-1} (b), and by adding 10^{-5} mbar of N$_2$ collision gas into the octopole (c). The mass spectrum (a) reveals that fragmentation of the n = 2 cluster into the m = 1 channel arising from metastable decay is minor, indicating that the [BZ-(H$_2$O)$_n$]H$^+$ clusters probed in the octopole are relatively cold. The mass spectrum (b) shows that resonant LID leads mainly to the loss of a single water molecule. Mass spectrum (c)

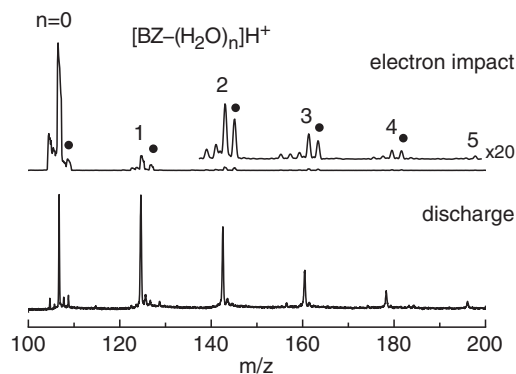FIG. 2. Mass spectra of [BZ-(H$_2$O)$_n$]H$^+$ clusters in the mass range m/z 100–200 produced in the electron impact (top) and plasma discharge (bottom) sources. Signals from protonated water clusters, (H$_2$O)$_n$H$^+$, are indicated by filled circles.

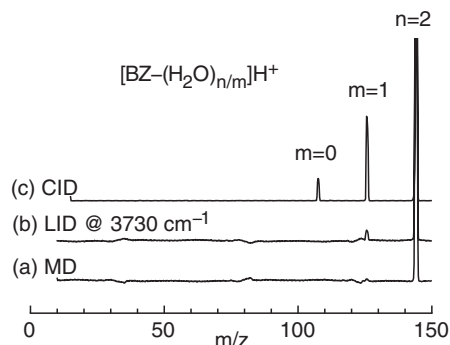FIG. 3. Mass spectra obtained by mass selecting $[BZ-(H_2O)_2]H^+$ generated in the electron impact source with the first quadrupole (m/z 143) and scanning the second quadrupole without laser excitation (a), with resonant IR excitation at $\nu_{IR} = 3730$ cm^{-1} (b), and with 10^{-5} mbar of N$_2$ collision gas in the octopole (c). While there is essentially no fragmentation from metastable decay (MD) of the selected $[BZ-(H_2O)_2]H^+$, LID generates fragments with m = 1 (loss of one ligand). CID produces fragments with m = 0 and 1. No $(H_2O)_mH^+$ fragments are observed in any of the mass spectra.

displays additional fragmentation into m = 0 and 1 arising from collision-induced dissociation (CID). The latter spectrum also confirms the composition of the m/z 143 ion as 107^+-$(H_2O)_2$, in line with $[BZ-(H_2O)_2]H^+$. The minor contribution of fragment ions produced by metastable decay is separated from the desired LID signal by triggering the ion source at twice the laser frequency (10 Hz) and subtracting signals from alternating triggers. All IRPD spectra obtained for n = 1–5 are compared in Fig. 4. The widths of the narrowest transitions are ~15 cm^{-1} and result from a combination of unresolved rotational substructure, possible contribution of several isomers, and thermal broadening due to sequence hot band transitions. The latter arises from the fact that the IR photon energy (<45 kJ/mol) is smaller than the ligand binding energies (at least for small n). As the moderate available laser intensity merely allows for single-photon IRPD processes,[9,14]
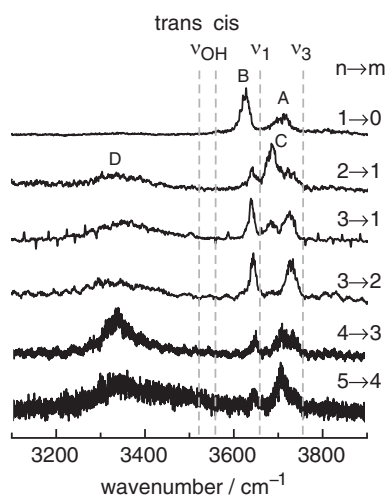

FIG. 4. IRPD spectra of $[BZ-(H_2O)_n]H^+$ clusters (n ≤ 5) recorded in the $[BZ-(H_2O)_m]H^+$ fragment channel (indicated as n → m). The positions, widths, and suggested vibrational assignment of the observed transitions are listed in Table II. The experimental frequencies of bare H$_2$O ($\nu_1 = 3657$ cm^{-1}, $\nu_3 = 3756$ cm^{-1})[43] and cis/trans-BZH$^+$ ($\nu_{OH} = 3555/3525$ cm^{-1})[11] are indicated by dashed lines.

only cluster ions with a certain amount of initial internal energy may be detected in the IRPD spectra.

B. Electronic spectroscopy

Electronic photodissociation spectra of mass-selected $[BZ-(H_2O_n)]H^+$ ions with n ≤ 2 are recorded in a reflectron time-of-flight mass spectrometer (ReTOF-MS).[4,7] $[BZ-(H_2O)_n]H^+$ clusters are generated in a pulsed high-voltage electrical discharge source coupled to a pulsed nozzle with 200 μm diameter. The discharge is produced 2 mm downstream from the nozzle orifice between two electrodes. The expanding gas mixture is obtained by passing 50% H$_2$ in He at a backing pressure of 4 bars through reservoirs filled with benzaldehyde and water at room temperature. The mass spectrum of this discharge source (Fig. 2) indicates efficient protonation and hydration of BZ. After passing through a skimmer, the ions are extracted into the ReTOF-MS with a resolution (m/Δm>200) sufficient to separate $[BZ-(H_2O)_n]H^+$ from BZ^+-$(H_2O)_n$ for the considered size range. LID of the ions is carried out in a 2 cm long interaction region located just before the reflectron mirror. The employed VIS-OPO laser is pumped by a Q-switched ns Nd:YAG laser operating at 10 Hz and produces tunable radiation between 385 and 670 nm with a pulse energy of 1–15 mJ at a bandwidth of 5 cm^{-1}. The laser beam is focused to about 1 mm^2 when interacting with the ion beam. Even at the minimal laser power required to detect the LID signal, its laser power dependence indicates some saturation (power dependence around I$^{0.5}$). The ReTOF-MS is set to detect neutral fragments on the first detector located behind the reflectron mirror, whereas all ions (parents and fragments) are repelled to the second detector. The LID spectrum is obtained by monitoring the neutral fragments as a function of the laser frequency. Neutral fragments produced by CID in the field-free region of the ReTOF-MS are discriminated from those produced by LID by accelerating the parent ions to 2 kV in the interaction region. As neutral LID fragments have the same kinetic energy as the parent ions, they are faster than those produced by CID in the field-free region and arrive earlier at the detector. As the interaction region is short compared to the field-free region, the CID fragments produced in the former region can be neglected.

C. Computational techniques

Quantum chemical calculations at the B3LYP/6-311++G(d,p) and MP2/cc-pVDZ levels are carried out using GAUSSIAN09,[28] to characterize the intermolecular potential energy surface, including the structures, energies, and vibrational properties of the various conformations of $[BZ-(H_2O)_n]H^+$ in their ground electronic state (S$_0$). All coordinates are relaxed during the search for stationary points, and the identification of minima is ensured by harmonic vibrational frequency analysis. All binding energies are corrected for unscaled zero-point vibrational energies and basis set superposition error. Harmonic frequencies obtained at the B3LYP level are scaled by a factor of 0.9578 to optimize the agreement between calculated and reported O–H stretch frequencies of bare H$_2$O ($\nu_1 = 3657$ cm^{-1}, ν_3

= 3756 cm^{-1}).[29] The charge distribution is evaluated by a natural bond orbital (NBO) analysis.

Additional calculations are performed at the ri-CC2/aug-cc-pVDZ level using TURBOMOLE 6.1 to probe the properties of the S_1 ($\pi\pi^*$) excited state and to simulate vibronic $S_1 \leftarrow S_0$ spectra.[30] Adiabatic S_1 excitation energies are corrected for zero point energy (ZPE). Multidimensional Franck-Condon simulations of $S_1 \leftarrow S_0$ spectra are carried out using PGOPHER and harmonic vibrational frequencies obtained at the ri-CC2/aug-cc-pVDZ level for both electronic states.[31] This procedure yielded vibronic $S_1 \leftarrow S_0$ spectra for BZH$^+$-L dimers with L = Ar and N$_2$ in quantitative agreement with their measured spectra.[10]

III. RESULTS AND DISCUSSION

A. [BZ-H$_2$O]H$^+$ dimer (n = 1)

An extensive search on the [BZ-H$_2$O]H$^+$ potential at the MP2 level resulted in several low-energy minima for the cis-BZH$^+$ and trans-BZH$^+$ isomers, denoted cw1-x and tw1-x and shown in Figs. 1 and S1 in the supplementary material for x ≤ 6.[45] All of them have the excess proton localized on the BZH$^+$ moiety. In line with previous calculations,[7,11,21,22] cis-BZH$^+$ is calculated to be 7 kJ/mol more stable than trans-BZH$^+$. The most stable BZH$^+$-H$_2$O dimers correspond to the H-bonded isomers, cw1-1 and tw1-1, with C$_s$ symmetry and nearly linear O–H···O H-bonds between the OH proton of BZH$^+$ and the oxygen atom of H$_2$O. The global minimum, cw1-1, is characterized by a H-bond length of 1.48 Å and a binding energy of 85 kJ/mol. Clearly, the charge is mostly localized on the cis-BZH$^+$ moiety, with only a minor charge transfer of 72 me to the H$_2$O ligand (Fig. S2 in the supplementary material).[45] In the slightly less stable local minimum, tw1-1, H$_2$O binds to trans-BZH$^+$ with a longer H-bond (1.54 Å) and a lower binding energy of 76 kJ/mol. Similar to the Ar and N$_2$ complexes,[10] the deviation of the H-bond from linearity in tw1-1 (169°) is larger than for cw1-1 (175°) due to steric hindrance arising from repulsion with the CH hydrogen atom in ortho position. In the significantly less stable isomers, cw1-2 and tw1-2 (Fig. S1 in the supplementary material),[45] the H$_2$O ligand interacts in bifurcated C–H···O H-bonds with the protons of the aromatic C–H group in ortho position and the methine C–H group (41 kJ/mol). Further less stable local minima (cw1-x/tw1-x with x = 3–6, Fig. S1 in the supplementary material)[45] feature weak bifurcated C–H···O H-bonds between two adjacent aromatic C–H groups of BZH$^+$ and H$_2$O (24–28 kJ/mol), as was observed in the benzene$^+$-H$_2$O cation.[18,32,33] Other conceivable structures, in which H$_2$O binds to the aromatic π electron system of the BZH$^+$ ring, are not identified as local minima. All efforts to locate π-bonded minima[32,34] converged to either the cw1-1 or tw1-1 minima, indicating that there is no (or only a low) barrier for $\pi \rightarrow$ OH isomerization. As the O–H···O H-bonded structures cw1-1 and tw1-1 are substantially more stable (>35 kJ/mol) than all other local minima, they are expected to be the dominant carriers of the measured IRPD spectrum. The population of the higher-lying local minima in the molecular beam is expected to be negligible and thus

not considered further. This procedure is also justified by the analysis of the measured IRPD spectrum outlined below.

No stable H$_3$O$^+$-BZ structure with an O–H...O H-bonded configuration has been found on the potential energy surface, in line with the much higher PA of BZ, which exceeds the one of H$_2$O by 144 kJ/mol (Table I). All H-bonded H$_3$O$^+$-BZ geometries optimize to BZH$^+$-H$_2$O structures indicating that the potential for intracluster proton transfer along the O–H...O coordinate is barrierless. Interestingly, there is a stable high-energy π-bonded H$_3$O$^+$-BZ isomer, in which the hydronium ion forms a π H-bond to the aromatic π-electron system of BZ (Fig. S3 in the supplementary material).[45] Such structures have previously been predicted[35] and spectroscopically observed[36] for complexes between H$_3$O$^+$ and benzene, as well as for H$_5$O$_2^+$-naphthalene.[8] The H$_3$O$^+$-BZ(π) isomer is 130 kJ/mol higher in energy than the cw1-1 isomer of cis-BZH$^+$-H$_2$O. Moreover, the intermolecular π H-bond in H$_3$O$^+$-BZ(π) is much weaker than the σ H-bond in cw1-1. Thus, the formation of H$_3$O$^+$-BZ(π) in the supersonic plasma expansion is not expected and this scenario is confirmed by the IR spectra analyzed below. Hence, we do not consider the π-bonded H$_3$O$^+$-BZ(π) isomer and its larger water adducts in detail further.

The IRPD spectrum of [BZ-H$_2$O]H$^+$ monitored in the H$_2$O loss channel is shown in Fig. 5, and the positions, widths, and suggested vibrational and isomer assignments are listed in Table II. CID and resonant LID of [BZ-H$_2$O]H$^+$ exclusively produce BZH$^+$ fragment ions. No H$_3$O$^+$ fragment ions are observed, in line with H$_2$O plus BZH$^+$ being the lowest-energy dissociation channel. In the investigated range, the [BZ-H$_2$O]H$^+$ spectrum displays only two transitions B and A at 3625 and 3709 cm^{-1}, which are readily assigned to the symmetric and antisymmetric O–H stretch modes of the H$_2$O ligand (ν_1, ν_3) acting as a proton acceptor in a BZH$^+$-H$_2$O configuration with favorable charge-dipole orientation. The observed redshifts, $\Delta\nu_1 = -32$ cm^{-1} and $\Delta\nu_3 = -47$ cm^{-1},
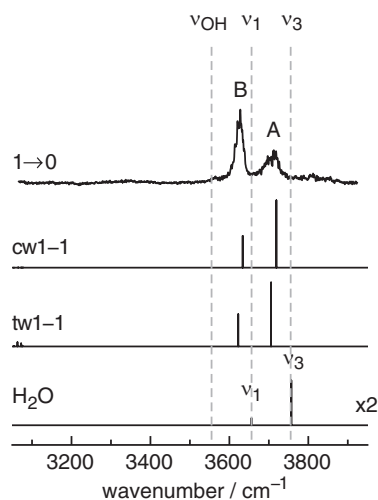

FIG. 5. IRPD spectrum of [BZ-H$_2$O]H$^+$ in the O–H stretch range monitored in the BZH$^+$ mass channel compared to linear IR absorption stick spectra of the cw1-1 and tw1-1 isomers of BZH$^+$-H$_2$O and H$_2$O obtained at the B3LYP/6-311++G(d,p) level (Table III). The experimental frequencies of bare H$_2$O (ν_1 = 3657 cm^{-1}, ν_3 = 3756 cm^{-1})[43] and cis-BZH$^+$ (ν_{OH} = 3555 cm^{-1})[11] are indicated by dashed lines.

TABLE II. Positions, widths (FWHM, in parenthesis), and suggested vibrational and isomer assignments of the transitions observed in the IRPD spectra of [BZ-$(H_2O)_n$]H$^+$ recorded in the [BZ-$(H_2O)_m$]H$^+$ fragment channel (Fig. 4).

n	n → m	Position (cm^{-1})	Vibration	Isomer[a]
1	1 → 0	A 3709 (38)	ν_3	cw1-1
		B 3625 (27)	ν_1	cw1-1
2	2 → 1	A 3730 (25)	ν_3	cw2-1
		C 3684 (24)	ν_f	cw2-1
		B 3640 (10)	ν_1	cw2-1
		D ~3340 (broad)	ν_b	cw2-1
3	3 → 2	A 3728 (23)	ν_3	cw3-1/cw3-2
		B 3643 (15)	ν_1	cw3-1/cw3-2
		D ~3320 (broad)	ν_b	cw3-2
	3 → 1	A 3723 (26)	ν_3	cw3-1/cw3-2
		C 3686 (23)	ν_f	cw3-2
		B 3640 (13)	ν_1	cw3-1/cw3-2
		D ~3350 (broad)	ν_b	cw3-2
4	4 → 3	A 3733 (12)	ν_3	cw4-1/cw4-2/cw4-3
		C 3706 (17)	ν_f	cw4-2/cw4-3
		B 3647 (13)	ν_1	cw4-1/cw4-2/cw4-3
		D ~3340 (broad)	ν_b	cw4-2/cw4-3

[a]Only assignments to cis isomers are listed. It is likely that some signal arises from the less stable trans isomers.

from the bare H_2O transitions at $\nu_1 = 3657$ and $\nu_3 = 3756$ cm^{-1} (indicated by dashed lines in Fig. 5) are similar to those previously observed for A(H)$^+$-H_2O complexes of related aromatic cations.[15,32–34,37] Moreover, they compare favorably with the values of $\Delta\nu_1 = -22$ and -38 cm^{-1} and $\Delta\nu_3 = -34$ and -51 cm^{-1} predicted for cw1-1 and tw1-1, respectively (Fig. 5 and Table III). These redshifts reflect the slight elongation of the O–H bonds of H_2O upon H-bonding to the BZH$^+$ cation ($\Delta r_{OH} = 5$ mÅ). The IR spectra calculated for cw1-1 and tw1-1 in the free O–H stretch range are similar and within experimental resolution compatible with the measured IRPD spectrum (Fig. 5). The large widths of ~30 cm^{-1} (FWHM) for the bands in the measured spectrum do not allow for a distinction between cis-BZH$^+$-H_2O and trans-BZH$^+$-H_2O. Hence, the observed bands are assigned to overlapping transitions of both cw1-1 and tw1-1, based on the previous observation of both isomers in BZH$^+$-L$_n$ clusters with L = Ar and N$_2$ generated in the same ion source,[11] and the similar stabilities of both monomers (PA) and their H-bond energies to H_2O. However, in line with previous conclusions, the more stable cis isomers are expected to dominate the population of both the BZH$^+$ and BZH$^+$-H_2O ions. The free O–H stretch fundamental of isolated cis/trans-BZH$^+$ has been inferred as $\nu_{OH} = $~3555/3525 cm^{-1}.[11] No signal is detected in this spectral range for [BZ-H_2O]H$^+$, confirming that H_2O is indeed H-bonded to the OH group of BZH$^+$ and not to any other binding site, i.e. the presence of any of the cw1-x and tw1-x isomers with x = 2–6 can be excluded. The strong H-bond leads to a large O–H bond elongation in BZH$^+$ ($\Delta r_{OH} \sim 50$ Å), accompanied by large redshifts of $\Delta\nu_{OH} = -857$ and -735 cm^{-1} and substantial enhancements in the IR intensities (factors of 9 and 15) predicted for cw1-1 and tw1-1, respectively (Table III). Thus, the intense ν_{OH} transitions of these isomers predicted at 2730/2817 cm^{-1} oc-

TABLE III. O–H stretch frequencies (in cm^{-1}) of various [BZ-$(H_2O)_n$]H$^+$ isomers compared to those of $(H_2O)_n$.[a]

Isomer	ν_{OH}	Assignment
cis-BZH$^+$	3587 (477)	ν_{OH}^f (BZH$^+$)
trans-BZH$^+$	3552 (127)	ν_{OH}^f (BZH$^+$)
cw1-1	3719 (171)	ν_3
	3634 (81)	ν_1
	2730 (4102)	ν_{OH}^b (BZH$^+$)
tw1-1	3706 (162)	ν_3
	3622 (82)	ν_1
	2817 (1904)	ν_{OH}^b (BZH$^+$)
cw2-1	3741 (138)	ν_3
	3696 (133)	ν_f
	3650 (44)	ν_1
	3217 (1185)	ν_b
	2131 (5868)	ν_{OH}^b (BZH$^+$)
tw2-1	3741 (134)	ν_3
	3696 (125)	ν_f
	3650 (46)	ν_1
	3203 (1196)	ν_b
	2332 (2956)	ν_{OH}^b (BZH$^+$)
cw3-1	3742 (293)/3741 (5)	ν_3
	3651 (34)/3651 (64)	ν_1
	3073 (787)/3072 (138)	ν_{OH}^b (H$_3$O$^+$)
	3042 (2220)	ν_{OH}^b (H$_3$O$^+$)
cw3-2	3748 (125)	ν_3
	3719 (108)	ν_f
	3697 (125)	ν_{OH}^f (H$_3$O$^+$)
	3655 (32)	ν_1
	3364 (804)	ν_b
	2895 (1916)	ν_{OH}^b (H$_3$O$^+$) to H_2O
	1712 (2934)	ν_{OH}^b (H$_3$O$^+$) to BZ
cw4-1	3739 (170)/3736 (133)	ν_3
	3706 (122)	ν_f
	3648 (42)/3645 (48)	ν_1
	3091 (680)/3064 (2133)	ν_{OH}^b (H$_3$O$^+$) to single H_2O
	2895 (2910)	ν_b(H_2O) to BZ
	1873 (3658)	ν_{OH}^b (H$_3$O$^+$) to H_2O-BZ
cw4-2	3746 (131)/3744 (147)	ν_3
	3719 (118)	ν_f
	3654 (35)/3652 (50)	ν_1
	3307 (938)	ν_b
	3044 (1349)/2610 (1874)/2445 (4818)	ν_{OH}^b (H$_3$O$^+$)
H_2O	3757 (57)	ν_3
	3656 (9)	ν_1
$(H_2O)_2$	3750 (86)	ν_3
	3729 (80)	ν_f
	3654 (16)	ν_1
	3550 (332)	ν_b

[a]B3LYP/6-311++G(d,p) level (IR intensities in km/mol are listed in parentheses).

cur outside of the spectral range investigated. For comparison, the measured H-bond induced redshifts in weakly bound cis-BZH$^+$-Ar/N$_2$ clusters were reported as $\Delta\nu_{OH} = -99/-215$ cm^{-1}, respectively.[11] Comparison of the IRPD spectrum measured for [BZ-H_2O]H$^+$ with the IR spectrum calculated for the high-energy H$_3$O$^+$-BZ(π) isomer (Fig. S3 in the supplementary material)[45] indicates that the latter does not contribute to the observed spectrum and its abundance is below the detection limit.
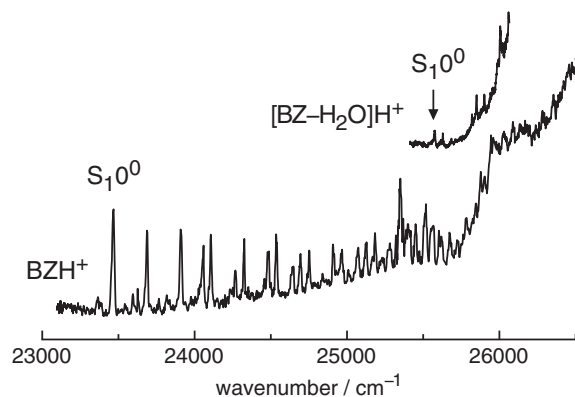
FIG. 6. Photofragmentation spectrum of the $S_1 \leftarrow S_0$ transition of [BZ-(H_2O)]H$^+$ compared to that of BZH$^+$ (Ref. 7). No signal is detected below the S_1 origin of [BZ-(H_2O)]H$^+$ down to 23 450 cm^{-1}.

The dissociation energies calculated for cis/trans-BZH$^+$-H_2O (85 and 76 kJ/mol for cw1-1 and tw1-1) are significantly larger than the IR photon energies employed for IRPD (hν < 50 kJ/mol). As the low photon flux achieved by the employed IR laser allows only for single-photon absorption,[9,14] dissociation of the clusters cannot occur from their ground vibrational state but only from vibrationally excited states. Thus, a large part of the widths of the bands arises from cross anharmonicities of the excited sequence hot band transitions giving rise to the signals observed in the IRPD spectrum.

The electronic photofragmentation spectrum of [BZ-(H_2O)]H$^+$ recorded in the vicinity of the S_1 origin of BZH$^+$ is compared in Fig. 6 to the vibronic $S_1 \leftarrow S_0$ spectrum of bare BZH$^+$ recorded previously in the same setup.[7] The S_1 origin observed for BZH$^+$ at 23 470 cm^{-1} was assigned to the lowest $\pi\pi^*$ transition of the cis-BZH$^+$ isomer by comparison to ri-CC2/aug-cc-pVDZ calculations (23 768 cm^{-1}).[10] The corresponding S_1 origin of the less abundant trans-BZH$^+$ isomer is predicted at much higher energy, around 0.2 eV (1467 cm^{-1}) above the S_1 origin of cis-BZH$^+$. Interestingly, the lowest singlet state in neutral BZ corresponds to $n\pi^*$ excitation at 26 918 cm^{-1} (S_1),[38] while the lowest

$\pi\pi^*$ excitation occurs at much higher energy (35 191 cm^{-1}, S_2).[39] However, protonation of BZ stabilizes the n orbital by ~10 eV, so that the $\pi\pi^*$ state at 23 470 cm^{-1} becomes the S_1 state in BZH$^+$.[7] The large redshift of the $\pi\pi^*$ state (11 721 cm^{-1}) upon protonation of BZ reflects directly the increase of the PA of cis-BZH$^+$ upon electronic excitation. By comparison with the BZH$^+$ spectrum, the first vibronic band observed in the [BZ-H_2O]H$^+$ spectrum at 25 576 cm^{-1} is assigned to the S_1 origin of cis-BZH$^+$-H_2O (cw1-1). No signal was detected to the red of this S_1 origin (down to 23 450 cm^{-1}). A few low-frequency vibrations are resolved before the spectrum becomes severely congested toward higher energies (>25 750 cm^{-1}), with a continuous background that could not be suppressed. Possible explanations for the background include the presence of hot ions together with cold ions in the volume probed by the laser and saturation effects (Sec. II B). Unfortunately, it was impossible to obtain sufficient LID signal by keeping the laser power dependence in the linear regime. As a consequence, weakly Franck-Condon allowed transitions may be excited and contribute to spectral congestion. Although the possibility of the simultaneous formation of several isomers cannot be ruled out completely, the IRPD spectra suggest the contribution of only the cw1-1 isomer in this spectral range. In particular, the S_1 origin of tw1-1 is predicted at significantly higher energy.

The S_1 origin observed for cis-BZH$^+$-H_2O is substantially blueshifted compared to bare cis-BZH$^+$. The spectral shift of $\Delta S_1 = 2106$ cm^{-1} corresponds directly to the change in intermolecular binding energy upon electronic excitation, i.e. the H-bond in cis-BZH$^+$-H_2O is less stable in the S_1 state by 2106 cm^{-1} (25.2 kJ/mol) compared to the ground state. Assuming the calculated binding energy of 85.2 kJ/mol in S_0, excitation into the S_1 state reduces the H-bond strength by 30%. Similar but smaller ΔS_1 blueshifts of 300 and 628 cm^{-1} are observed for cis-BZH$^+$-L dimers with L = Ar and N_2.[10] Table IV and Fig. 7 compare the ΔS_1 shifts measured for cis-BZH$^+$-L with those predicted at the ri-CC2/aug-cc-pVDZ level. The good agreement between experimental and calculated shifts confirms the given isomer assignments. Moreover, the ΔS_1 shifts show a strong correlation with the proton

TABLE IV. Vertical and adiabatic transition energies for $S_1 \leftarrow S_0$ ($\pi\pi^*$) excitation ($E_{vert/ad}$ in cm^{-1}) of cis-BZH$^+$-L_n clusters and oscillator strength calculated at the ri-CC2/aug-cc-pVDZ level compared to experimental values (in cm^{-1}). Values for BZ and trans-BZH$^+$ are listed for comparison.

| Species	E_{vert} (calc)	E_{ad} (calc)	E_{ad} (expt)	Oscillator strength[a]
BZ	30 123 ($n\pi^*$, S_1)	25 157 ($n\pi^*$, S_1)	26 918[b]	0.00017
	38 304 ($\pi\pi^*$, S_2)	34 838 ($\pi\pi^*$, S_2)	35 191[c]	0.012
cis-BZH^{+}[d]	27 933	23 768	23 470	0.0296
trans-BZH$^+$	29 162	25 235	…	0.0307
cis-BZH$^+$-Ar[d]	28 125	24 010	23 770	0.0295
cis-BZH$^+$-N_2[d]	28 461	24 356	24 098	0.0293
cis-BZH$^+$-H_2O (cw1-1)	29 685	25 797	25 576	0.0295
cis-BZH$^+$-$(H_2O)_2$ (cw2-1)	30 725	26 948	…	0.0291
cis-BZH$^+$-$(H_2O)_3$ (cw3-1)	33 734	28 552	…	0.0251
cis-BZH$^+$-$(H_2O)_4$ (cw4-2)	34 448	29 462	…	0.0261

[a]Vertical transition.
[b]Reference 38.
[c]Reference 39.
[d]Reference 10.
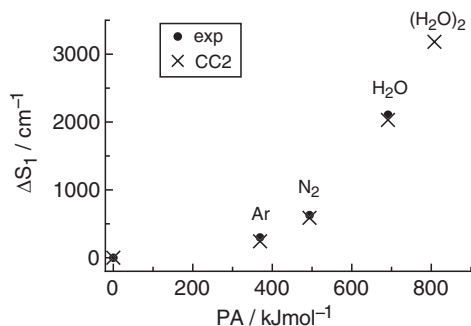
FIG. 7. Experimental and calculated ΔS_1 shifts of cis-BZH$^+$-L$_n$ as a function of the proton affinity of L$_n$. Calculated values are obtained at the ri-CC2/aug-cc-pVDZ level (Table IV).

FIG. 8. Franck-Condon simulation of the $S_1 \leftarrow S_0$ transition of the cw1-1 isomer of BZH$^+$-H$_2$O at T = 0 K (top) compared to the experimental spectrum of [BZ-H$_2$O]H$^+$ (Table V). The energy scale is relative to the $S_1 \leftarrow S_0$ origin band. The simulated spectrum is convoluted with a Gaussian line shape with a FWHM of 6 cm^{-1}. Progressions in the intermolecular in-plane bending frequency (β') are indicated. To facilitate convenient comparison with the calculated spectrum, the rising background of the measured spectrum was subtracted (Fig. 6).

affinity of the ligand. The weaker H-bonds in the S_1 states of the BZH$^+$-L dimers result from a substantial increase in the PA of BZ upon electronic excitation, i.e. the OH group in BZH$^+$ is much less acidic in S_1 as compared to S_0.

The ri-CC2 calculations provide further insight into the impact of S_1 excitation on the structural, vibrational, and electronic properties of cis-BZH$^+$-H$_2$O. The predicted S_1 origin at 25 797 cm^{-1} and ΔS_1 blueshift of 2029 cm^{-1} agree well the measured values (25 576 and 2106 cm^{-1}). The $S_1 \leftarrow S_0$ transition has 95% HOMO-LUMO character ($\pi\pi^*$) and the corresponding molecular orbitals are depicted in Fig. S4 in the supplementary material.[45] As for cis-BZH$^+$,[10] the HOMO (π) is mostly localized on the aromatic ring, while the LUMO (π^*) is distributed also over the protonated formyl group. Hence, the $S_1 \leftarrow S_0$ transition has intramolecular charge transfer character, and an overall electron density of 0.35 e is transferred from the aromatic ring to the CHOH group,[7] giving rise to the reduction in the H-bond interaction.

The structural parameters of cw1-1 in the S_0 and S_1 state are summarized in Fig. S5 in the supplementary material.[45] The complex has in both electronic states a cis-BZH$^+$-H$_2$O configuration. As the intermolecular bond is weaker in the S_1 state, the H-bond to H$_2$O elongates by 112 mÅ and the intramolecular O–H bond of cis-BZH$^+$ contracts by 25 mÅ. S_1 excitation also changes the geometry of the aromatic ring from a regular hexagon to a more quinoidal-like structure. Because the LUMO (π^*) orbital is also partly localized on the protonated formyl group, S_1 excitation has a drastic effect on its geometry, with large elongations of the C–O (52 mÅ) and C–C bonds (35 mÅ) and large changes in the bond angles (up to 3°) induced by changes in the hyperconjugation.

The structural modifications upon S_1 excitation of cw1-1 translate directly into changes in the vibrational frequencies and lead to excitation of the corresponding Franck-Condon (FC) active modes in the vibronic $S_1 \leftarrow S_0$ spectrum. The harmonic vibrational frequencies and normal coordinates obtained for the S_0 and S_1 states at the ri-CC2/aug-cc-pVDZ level (Table T1 in the supplementary material)[45] are employed in FC simulations of the $S_1 \leftarrow S_0$ vibronic spectrum of the cw1-1 isomer, in order to assign vibrational transitions observed in the measured spectrum of BZH$^+$-H$_2$O (Fig. 8). The six intermolecular modes are the intermolecular stretch (σ), the in-plane and out-of-plane bends (β', β'') and wags
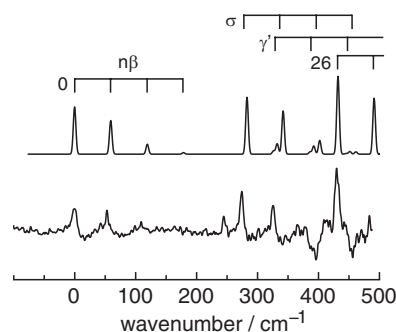
(γ', γ''), and the torsion (τ). The numbering of the 39 intramolecular modes (27a$'$ + 12a$''$) of cis-BZH$^+$ follows the Mulliken notation applied to the S_0 frequencies. Owing to the weaker H-bond in the excited state, σ decreases drastically from 377 cm^{-1} in S_0 to 283 cm^{-1} in S_1. Initial simulations reveal that – as expected for a planar complex – only the three in-plane intermolecular modes (β', γ', σ) are relevant. In addition, the low-frequency intramolecular in-plane mode ν_{26} predicted at 432 cm^{-1} has high FC activity, as this mode describes the large angular deformation of the protonated formyl group upon S_1 excitation. Progressions in ν_{26} are also observed in the S_1 spectra of cis-BZH$^+$ and its complexes with Ar and N$_2$.[7,10] The spectrum simulated for T = 0 K using a convolution width of 6 cm^{-1} compares favorably with the measured spectrum and allows for an assignment of the observed vibronic transitions (Table V and Fig. 8). Moreover, this good correspondence strongly supports the given isomer assignment of the experimental

TABLE V. Vibrational frequencies (in cm^{-1}) observed in the excitation spectrum of [BZ-H$_2$O]H$^+$ compared to calculated frequencies of FC-active modes in the S_1 state of cis-BZH$^+$-H$_2$O (cw1-1) obtained at the ri-CC2/aug-cc-pVDZ level (Fig. 8).

Experimental	Calculated	Assignment
53	59	β'
109	119	$2\beta'$
	178	$3\beta'$
245		
275	283	σ
	327	$2\nu_{39}$
318	333	γ'
325	342	$\sigma + \beta'$
376	392	$\gamma' + \beta'$
415	402	$\sigma + 2\beta'$
429	432	ν_{26}
	451	$\gamma' + 2\beta'$
	461	$\sigma + 3\beta'$
	492	$\nu_{26} + \beta'$

spectrum to cw1-1. Particularly striking are the long β' progressions (up to three quanta) in combination with the S_1 origin and other fundamentals. The σ value measured for cis-BZH$^+$-H$_2$O (275 cm^{-1}) is much higher than those of cis-BZH$^+$-L with L = Ar (60 cm^{-1}) and N$_2$ (94 cm^{-1}),[10] due to its much stronger H-bond and the lighter mass of the ligand. FC simulations conducted for variable temperatures in steps of 10 K suggest a vibrational temperature of less than 50 K for the cold population of BZH$^+$-H$_2$O ions in the molecular beam from the absence of any distinct hot band transition to the red of the S_1 origin in the measured spectrum. The HOMO and LUMO orbitals of cis-BZH$^+$-H$_2$O are similar to those of cis-BZH$^+$ (Fig. S4) consistent with the minor impact of H$_2$O on the orbitals localized on the aromatic molecule.

B. [BZ-(H$_2$O)$_2$]H$^+$ trimer (n = 2)

Further hydration of BZH$^+$-H$_2$O to form the BZH$^+$-(H$_2$O)$_2$ trimer may occur either by interior ion hydration via the separate attachment of two individual H$_2$O ligands to the BZH$^+$ ion core at two different binding sites or by the attachment of a H-bonded (H$_2$O)$_2$ dimer to BZH$^+$.[14,17,18] The latter scenario corresponds to the onset for the formation of an H-bonded solvent network. The global minimum structure corresponds to the cis-BZH$^+$-(H$_2$O)$_2$ structure, cw2-1, in which a H-bonded (H$_2$O)$_2$ dimer binds to the OH proton of cis-BZH$^+$ in a linear fashion (Fig. 1). The total interaction energy amounts to 138 kJ/mol. Both intermolecular bonds in cw2-1 are substantially stronger and shorter (1.296 and 1.610 Å) than those in the respective cis-BZH$^+$-H$_2$O and (H$_2$O)$_2$ dimer units (1.484 and 1.944 Å), indicating large and constructive three-body effects in this charged H-bonded network.[14,18] Again, the corresponding trans-BZH$^+$-(H$_2$O)$_2$ isomer, tw2-1, is somewhat less stable (121 kJ/mol) with correspondingly longer H-bonds (1.324 and 1.615 Å). As a consequence of the stronger intermolecular H-bonds, the intramolecular O–H bond in BZH$^+$ is lengthened by 93 and 85 mÅ in cw2-1 and tw2-1, respectively, upon attachment of the second H$_2$O ligand. Thus, the excess proton is shifted further toward the solvent cluster, although it is still closer to BZH$^+$ than to (H$_2$O)$_2$, e.g, 1.128 vs 1.296 Å in the case of cw2-1. This scenario is in line with the proton affinities of H$_2$O, (H$_2$O)$_2$, and BZ, which increase in the order is 690 < 808 < 834 kJ/mol. The proton initially attached to BZ shifts substantially toward the (H$_2$O)$_2$ solvent network by 151 mÅ. CID and LID (IRPD) experiments of mass selected [BZ-(H$_2$O)$_2$]H$^+$ ions (Fig. 3) result in the exclusive formation of [BZ-H$_2$O]H$^+$ and BZH$^+$ fragment ions. There is no evidence in the CID/LID experiments for the formation of the protonated solvent clusters, (H$_2$O)$_n$H$^+$ with n ≤ 2, consistent with the thermodynamic data. Hence, the successive loss of individual H$_2$O ligands or the loss of a (H$_2$O)$_2$ dimer unit are the lowest energy dissociation channels, whereas loss of BZ is not observed. All efforts to optimize structures of the type BZ-(H$_2$O)$_2$H$^+$ converge via barrierless proton transfer to the more stable BZH$^+$-(H$_2$O)$_2$ structures. Other structures of interior ion solvation, in which two individual H$_2$O ligands bind separately to different

binding sites of BZH$^+$ are also less stable and not observed in the IRPD spectrum of [BZ-(H$_2$O)$_2$]H$^+$.

The IRPD spectrum of [BZ-(H$_2$O)$_2$]H$^+$ recorded in the water loss channel is presented in Fig. 9, and the positions, widths, and suggested vibrational assignments are listed in Table II. The spectrum exhibits three transitions in the free O–H stretch range (A-C) and a considerably redshifted broad absorption (D) in the 3000–3400 cm^{-1} range. The bands B and A at 3640 and 3730 cm^{-1} are assigned to free ν_1 and ν_3 modes of the terminal H$_2$O ligand in BZH$^+$-(H$_2$O)$_2$ clusters as shown in Fig. 1. Their redshifts of $\Delta\nu_1 = -17$ and $\Delta\nu_3 = -26$ cm^{-1} from the transitions of bare H$_2$O and blueshifts of $\Delta\nu_1 = 15$ and $\Delta\nu_3 = 21$ cm^{-1} from BZH$^+$-H$_2$O are consistent with the predicted shifts. These shifts are in line with the calculated O–H bond lengths, which increase in the order H$_2$O < cis-BZH$^+$-(H$_2$O)$_2$ < cis-BZH$^+$-H$_2$O (0.965 < 0.968 < 0.970 Å). The transition at 3684 cm^{-1} is readily assigned to the free O–H stretch mode (ν_f) of the bound H$_2$O molecule in the BZH$^+$-(H$_2$O)$_2$ trimer, whereas the broad absorption centered at 3340 cm^{-1} is the spectroscopic fingerprint of the bound O–H stretch mode (ν_b) of the H-bonded (H$_2$O)$_2$ dimer attached to BZH$^+$. Similar spectral pattern have been reported in complexes of related aromatic cations hydrated by (H$_2$O)$_2$, indicating that the excess proton remains on BZH$^+$ in a BZH$^+$-(H$_2$O)$_2$ configuration.[14,17,18] The structural changes induced by addition of the second water molecule translate directly into the IR spectral properties of BZH$^+$-(H$_2$O)$_2$. The bound O–H stretch frequencies of BZH$^+$ in cw2-1 (2232 cm^{-1}) and tw2-1 (2136 cm^{-1}) are strongly redshifted due to strong H-bonds between BZH$^+$ and (H$_2$O)$_2$. These values are much lower than for BZH$^+$-H$_2$O (2730 and 2817 cm^{-1}), confirming the increased proton shift toward the solvent upon attachment of the second H$_2$O ligand. In addition, the bound O–H stretch frequency of the (H$_2$O)$_2$ unit in cw2-2 and tw2-2, $\nu_b = 3217$ and 3203 cm^{-1}, is significantly lower than the one calculated for bare (H$_2$O)$_2$, $\nu_b = 3550$ cm^{-1}, which is a clear sign of the enhanced H-bond strength in the solvent cluster upon attachment of BZH$^+$. As for the dimer, the IR spectra of the cw2-1 and tw2-1 trimer isomers are similar, and the measured IRPD
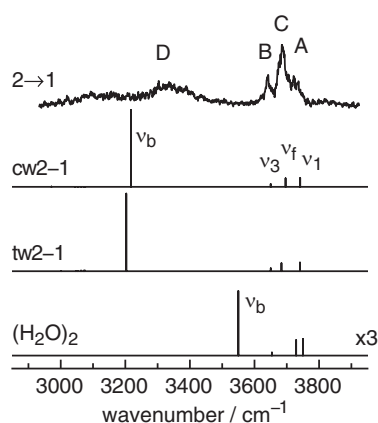
FIG. 9. IRPD spectrum of [BZ-(H$_2$O)$_2$]H$^+$ in the O–H stretch range monitored in the BZH$^+$-H$_2$O mass channel compared to linear IR absorption stick spectra of the cw2-1 and tw2-1 isomers and (H$_2$O)$_2$ obtained at the B3LYP/6-311++G(d,p) level (Table III).

spectrum is not of sufficient spectral resolution to distinguish between them. Analysis of the NBO charges confirm the bonding situation in cis-BZH$^+$-(H$_2$O)$_2$ (Fig. S2 in the supplementary material).[45] The positive charge is still largely localized on the cis-BZH$^+$ (886 me) but the transfer of 114 me to the (H$_2$O)$_2$ solvent cluster is larger than for cis-BZH$^+$-H$_2$O (72 me). Within the (H$_2$O)$_2$ solvent in cw2-1, the first H$_2$O ligand carries more positive charge than the terminal one (77 and 37 me). Significantly, the IRPD spectrum of [BZ-(H$_2$O)$_2$]H$^+$ does not show any transition near the free O–H stretch band of isolated BZH$^+$, indicating that at least one H$_2$O ligand is attached to the OH proton of BZH$^+$ (Fig. 4).

In contrast to cis-BZH$^+$ and cis-BZH$^+$-H$_2$O, the electronic photofragmentation spectrum of mass-selected [BZ-(H$_2$O)$_2$]H$^+$ clusters produced in the discharge source does not show any resonant absorption in the 23 000–27 400 cm^{-1} range investigated. Thus, it is concluded that the S$_1$ origin is shifted outside this range upon the attachment of the second H$_2$O ligand. Indeed, the highly reliable calculations (vide infra) predict the S$_1$ origin of cis-BZH$^+$-(H$_2$O)$_2$ at 26 948 cm^{-1}, which corresponds to a large incremental blueshift of ΔS$_1$ = 1151 cm^{-1} from S$_1$ of cis-BZH$^+$-H$_2$O (Fig. 7, Table IV) and is close to the edge of the scanned range. Thus, the intermolecular bond of cis-BZH$^+$ to the (H$_2$O)$_2$ solvent is weakened and elongated by 153 mÅ (Fig. S6 in the supplementary material).[45] As a result, the excess proton shifts slightly backward (by 51 mÅ) to the BZ molecule in the S$_1$ excited state of BZH$^+$-(H$_2$O)$_2$. Furthermore, the intermolecular bond within the (H$_2$O)$_2$ solvent cluster is weakened and elongated by 153 mÅ upon S$_1$ excitation. It is unlikely that the excess proton is transferred from the BZH$^+$ to (H$_2$O)$_2$ moiety upon S$_1$ excitation because the PA of BZ increases in the S$_1$ state, which destabilizes the H-bond between cis-BZH$^+$ and (H$_2$O)$_2$ by 3180 cm^{-1} (38 kJ/mol) upon electronic excitation. As the excess proton remains with BZ, the HOMO and LUMO orbitals of cis-BZH$^+$-(H$_2$O)$_2$ are similar to those of bare cis-BZH$^+$ (Fig. S4 in the supplementary material).[45]

C. [BZ-(H$_2$O)$_3$]H$^+$ tetramer (n = 3)

Only possible isomers of the [BZ-(H$_2$O)$_3$]H$^+$ tetramer with a H-bonded (H$_2$O)$_3$ trimer solvent network attached to the aromatic molecule are considered in the search for stable geometries (Fig. 10). For structures with a BZH$^+$ ion core, only the cis-BZH$^+$-(H$_2$O)$_3$ isomers are investigated, because the trans isomers are less stable (and mostly have quite similar IR spectra). As the PA of (H$_2$O)$_3$ is substantially larger than the PA of BZ (879>834 kJ/mol), the proton is expected to be localized on the water network in the most stable [BZ-(H$_2$O)$_3$]H$^+$ clusters. Indeed, the global minimum structure identified in our search, cw3-1, is of the type [BZ-(H$_2$O)$_3$H$^+$] with a total interaction energy of 188.0 kJ/mol. In this Eigen-type structure with C$_s$ symmetry, each of the three protons of an H$_3$O$^+$ core ion is solvated by a neutral ligand (two H$_2$O and one BZ). The H-bonds to H$_2$O are weaker and longer than those to BZ

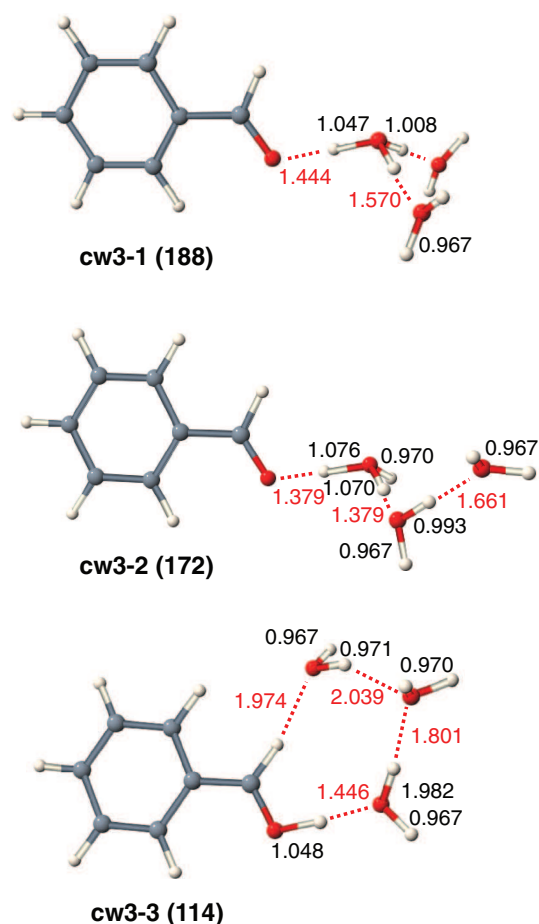
FIG. 10. Minimum energy structures of [BZ-(H$_2$O)$_3$]H$^+$ isomers calculated at the MP2/cc-pVDZ level. Bond lengths and total binding energies are given in Å and kJ/mol, respectively.

(1.570 vs 1.444 Å) due to its lower PA. As a consequence, the intramolecular donor O–H bonds of H$_3$O$^+$ toward the H$_2$O ligands are shorter than that toward Bz (1.008 vs. 1.047 Å). Clearly, the O$\cdots$H–O proton bridge between BZ and H$_3$O$^+$ is rather asymmetric (1.444 and 1.047 Å). The NBO analysis yields positive charges of 774, 49, and 128 me for H$_3$O$^+$, H$_2$O, and BZ, consistent with the notation of a threefold solvated hydronium ion (Fig. S2 in the supplementary material).[45]

The local minimum, cw3-2, has also a BZ-(H$_2$O)$_3$H$^+$ type structure and is 16 kJ/mol less stable than cw3-1. In cw3-2, the H$_3$O$^+$ core is twofold solvated by a BZ and a (H$_2$O)$_2$ dimer, leading to a chain-like solvent network. The O$\cdots$H–O proton bridge between BZ and H$_3$O$^+$ is slightly less asymmetric than in cw3-1, with bond lengths of 1.379 and 1.076 Å. Also, the intermolecular bond between H$_3$O$^+$ and (H$_2$O)$_2$ is stronger than the corresponding bond to a single H$_2$O ligand in cw3-1 (1.379 vs 1.570 Å). Again, the H-bond in the (H$_2$O)$_2$ ligand in cw3-2 is much stronger than in the bare (H$_2$O)$_2$ dimer, due to the presence of the nearby H$_3$O$^+$ ion.

All BZH$^+$-(H$_2$O)$_3$ structures with a BZH$^+$ core ion are found to be substantially less stable local minima. One such example is cw3-3, with a stabilization energy of 114 kJ/mol and a cyclic solvent structure, in which the protonated formyl

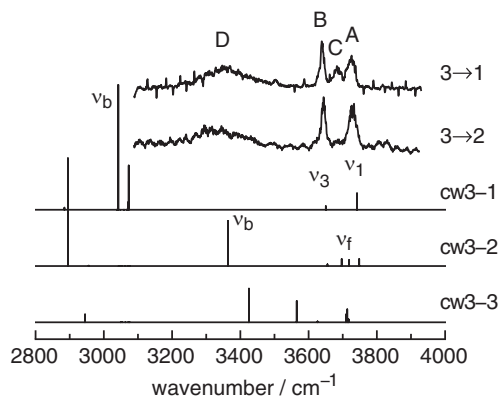FIG. 11. IRPD spectra of [BZ-(H$_2$O)$_3$]H$^+$ in the O–H stretch range monitored in the [BZ-(H$_2$O)$_2$]H$^+$ and [BZ-H$_2$O]H$^+$ mass channels (indicated as 3 → 2 and 3 → 1) compared to linear IR absorption stick spectra of the cw3-x (x = 1–3) isomers (Fig. 10) obtained at the B3LYP/6-311++G(d,p) level (Table III).

group acts as a OH and CH proton donor. Although this structure features the largest number of H-bonds, these are all rather weak, except for the asymmetric O–H$\cdots$O proton bridge between the OH proton of BZH$^+$ and the first H$_2$O ligand (1.048 and 1.446 Å).

The IRPD spectra of [BZ-(H$_2$O)$_3$]H$^+$ recorded in the one and two water loss channels (denoted 3 → 2 and 3 → 1) are shown in Fig. 11, and the positions, widths, and suggested vibrational assignments are listed in Table II. The 3 → 2 spectrum displays two sharper bands A and B at 3728 and 3643 cm^{-1} in the free O–H stretch range, which are assigned to ν_3 and ν_1 modes of H$_2$O ligands in [BZ-(H$_2$O)$_3$]H$^+$ that are merely proton acceptors in the H-bonded network. Their blueshifts of $\Delta\nu_{1/3}$ = 18/19 cm^{-1} compared to [BZ-H$_2$O]H$^+$ and redshifts of $\Delta\nu_{1/3}$ = −14/−28 cm^{-1} compared to bare H$_2$O confirm that both O–H bonds are free. Thus, these transitions are consistent with the global minimum, cw3-1, which has four essentially equivalent free OH groups of the two terminal H$_2$O ligands, with calculated ν_3 and ν_1 frequencies of 3742 and 3651 cm^{-1}, respectively. The O–H stretch frequencies of the three strongly H-bonded OH groups of the H$_3$O$^+$ ion of cw3-1 are predicted to be below 3100 cm^{-1} and thus outside the investigated spectral range (Table III). The broad intense transition centered near 3320 cm^{-1} in the IRPD spectrum is indicative of a bound O–H stretch (ν_b) of H-bonded H$_2$O ligands. Thus, this band cannot be rationalized by the cw3-1 global minimum structure but is indicative of isomers which contain neutral (H$_2$O)$_2$ dimer (or H$_2$O-BZ) units, such as cw3-2. The presence of both cw3-1 and cw3-2 isomers in the beam is strongly indicated by the 3 → 1 spectrum. It is different in appearance from the 3 → 2 spectrum and exhibits three rather than two distinct transitions in the free O–H stretch range. Two of them at 3723 and 3640 cm^{-1} are observed at similar positions as those in the 3 → 2 spectrum and assigned to ν_3 and ν_1 modes of H$_2$O ligands not acting as proton donors, which occur in both cw3-1 and c3w-2. The third band at 3686 cm^{-1} is clearly assigned to free O–H stretch modes (ν_f) of a H$_2$O ligand and/or H$_3$O$^+$ acting as a proton donor in H-bonds to other H$_2$O and BZ ligands. Thus, in addition to the broad

band near 3350 cm^{-1}, the 3686 cm^{-1} transition provides a further spectroscopic fingerprint of the cw3-2 isomer. Indeed the observed position of the latter band matches well the two frequencies of 3697 and 3719 cm^{-1} calculated for ν_f transitions of cw3-2. The broad band near ∼3350 cm^{-1} is slightly blueshifted and more intense than the corresponding transition in the 3 → 2 spectrum. In both cases, this transition is attributed to the ν_b mode of the cw3-2 isomer calculated as 3364 cm^{-1}. The ν_3 and ν_1 modes of cw3-1 and cw3-2 overlap in both spectra. In conclusion, the two [BZ-(H$_2$O)$_3$]H$^+$ spectra monitored in the one and two water loss channels (3 → 2 and 3 → 1) are explained by the two most stable isomers identified, cw3-1 and cw3-2, whereby the contribution of the cw3-2 isomer to the 3 → 1 spectrum is enhanced. This observation may be rationalized by the possible loss of an intact (H$_2$O)$_2$ dimer from cw3-2 by breaking only a single H-bond. Loss of two H$_2$O ligands from cw3-1 requires the rupture of two strong H-bonds and is thus energetically less favorable. No loss of neutral BZ ligands is observed upon IRPD and CID, suggesting that the H-bond energy of H$_3$O$^+$ to BZ is stronger than those to H$_2$O and (H$_2$O)$_2$, respectively, in line with the intermolecular bond distances of cw3-1 and cw3-2 in Fig. 10.

Significantly, the measured IRPD spectra of [BZ-(H$_2$O)$_3$]H$^+$ are not compatible with any spectra calculated for BZH$^+$-(H$_2$O)$_3$ type isomers, in which the excess proton is localized on the aromatic molecule (see Fig. 11 for the cw3-3 isomer). Thus, in line with the calculations, also the IRPD spectra of [BZ-(H$_2$O)$_n$]H$^+$ indicate that intracluster proton transfer from the aromatic molecule to the solvent cluster occurs in the ground electronic state at the critical solvation size of n ≥ n$_c$ = 3. Thus, while the excess proton in [BZ-(H$_2$O)$_3$]H$^+$ is localized on the solvent moiety, in the most stable IRPD fragment structures (m = 1 and 2) the proton is localized on BZH$^+$, suggesting that IRPD is accompanied by (barrierless) intracluster proton transfer.

Significantly, $\pi\pi^*$ excitation of the most stable cw3-1 isomer of [BZ-(H$_2$O)$_3$]H$^+$, which has a BZ-(H$_2$O)$_3$H$^+$ structure, leads to an electronically excited state, in which the proton is transferred back from the (H$_2$O)$_3$H$^+$ solvent to the BZ solute, i.e. it has a BZH$^+$-(H$_2$O)$_3$ type structure (Fig. S6 in the supplementary material).[45] This is readily rationalized by the largely enhanced PA of BZ in the $\pi\pi^*$ excited state. Geometry optimization starting from vertical excitations indicate barrierless proton transfer along the O–H$\cdots$O coordinate of cw3-1 in the $\pi\pi^*$ state, with a potential energy release of E$_{vert}$-E$_{ad}$ = 5182 cm^{-1} (Table IV). The origin transition is predicted at 28 552 cm^{-1}, i.e. shifted to the blue by 1604 cm^{-1} from the one predicted for the cw2-1 isomer of BZH$^+$-(H$_2$O)$_2$, which does not exhibit a proton transfer upon $\pi\pi^*$ excitation.

D. [BZ-(H$_2$O)$_4$]H$^+$ pentamer (n = 4)

Selected stable geometries of the [BZ-(H$_2$O)$_4$]H$^+$ pentamer are presented in Fig. 12, along with their total binding energies and relevant geometrical parameters. The excess proton is expected to be attached to the water solvent network in S$_0$, because the PA of (H$_2$O)$_4$ is 79 kJ/mol higher than
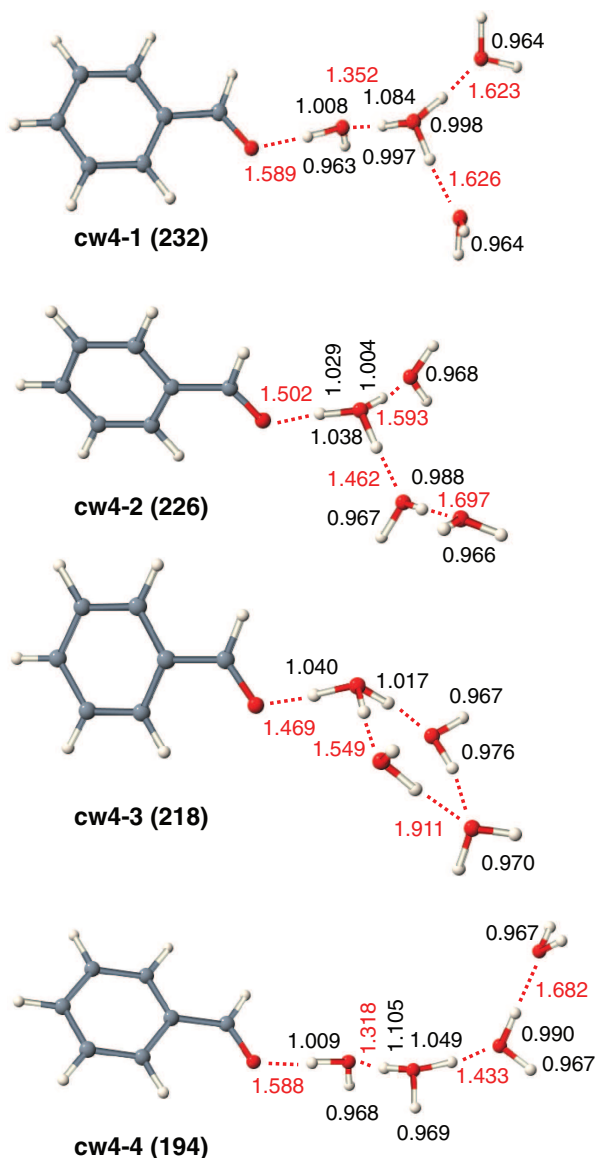
FIG. 12. Minimum energy structures of $[BZ\text{-}(H_2O)_4]H^+$ isomers calculated at the MP2/cc-pVDZ level. Bond lengths and total binding energies are given in Å and kJ/mol, respectively.

that of BZ (Table I). Indeed, all low-energy $[BZ\text{-}(H_2O)_4]H^+$ clusters have $BZ\text{-}(H_2O)_4H^+$ type geometries. Actually, most geometries considered in Fig. 12 are derived from initial geometries of an H-bonded $(H_2O)_4$ cluster attached to cis-BZH$^+$, which transform barrierless into proton-transferred structures upon the energy optimization process. The most stable structure found, cw4-1, with a total binding energy of 232 kJ/mol, is obtained by attaching the BZ molecule at the surface to a terminal H_2O ligand of the Eigen $H_9O_4^+$ ion, leading to a structure in which a central H_3O^+ core is solvated by three H_2O ligands without any direct contact to BZ. The H-bonds to the two single H_2O ligands are substantially weaker and longer than those to the $H_2O\text{-}BZ$ dimer. The slightly less stable cw4-2 isomer, with a total binding energy of 226 kJ/mol, is obtained by adding one H_2O molecule to a terminal H_2O ligand in cw3-1, leading to a structure in which a central H_3O^+ core is solvated by three neutral ligands, with H-bonds lengths increasing in the order $(H_2O)_2 < BZ < H_2O$

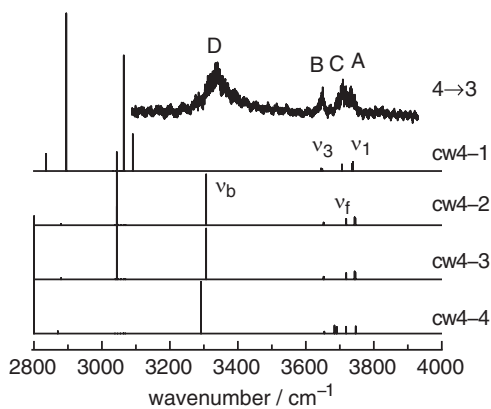FIG. 13. IRPD spectrum of $[BZ\text{-}(H_2O)_4]H^+$ in the O–H stretch range monitored in the $[BZ\text{-}(H_2O)_3]H^+$ mass channel compared to linear IR absorption stick spectra of the cw4-x (x = 1–4) isomers (Fig. 12) obtained at the B3LYP/6-311++G(d,p) level (Table III).

$(1.462 < 1.502 < 1.593$ Å). The O–H$\cdots$O bridge between the OH proton of H_3O^+ and BZ in cw4-2 is much more asymmetric (1.502 and 1.029 Å) than in cw3-1, clearly indicating the increasing tendency of the proton shift toward the solvent cluster with increasing hydration. Indeed, the NBO analysis for cw4-2 indicates that only 105 me remains on BZ. The somewhat less stable third $BZ\text{-}(H_2O)_4H^+$ structure shown in Fig. 12, cw4-3, features a cyclic $(H_2O)_4H^+$ solvation ring with a strong direct contact between H_3O^+ and BZ. The chain-like cw4-4 isomer is less favorable, because of the incomplete solvation of the H_3O^+ center.

The IRPD spectrum of $[BZ\text{-}(H_2O)_4]H^+$ monitoring the $[BZ\text{-}(H_2O)_3]H^+$ mass channel is presented in Fig. 13. No resonances are observed by monitoring the loss of BZ, suggesting that the bond to BZ is stronger than the weakest bond to H_2O, which is consistent with the bond lengths for all isomers in Fig. 12. The positions of the observed transitions along with their widths and suggested vibrational assignments are listed in Table II. Transitions B and A observed at 3647 and 3733 cm^{-1} are assigned to ν_1 and ν_3 of terminal H_2O ligands. Transition C at 3647 cm^{-1} is attributed to free O–H stretch modes (ν_f) of a H_2O ligand and/or H_3O^+ acting as a proton donor in H-bonds to other H_2O and BZ ligands, while the broad band D near 3340 cm^{-1} is due to a bound O–H stretch (ν_b) of a H_2O ligand with a free OH group and one H-bond to a neutral H_2O or BZ ligand. Thus, the bands C and D are characteristic for isomers cw4-2 and cw4-3, while bands A and B are consistent with all three low-energy structures.

Similarly to cw3-1, $\pi\pi^*$ excitation of the cw4-2 isomer of $[BZ\text{-}(H_2O)_4]H^+$ with a $BZ\text{-}(H_2O)_4H^+$ structure in S_0 leads to an excited state structure, in which the proton is transferred back in a barrierless reaction to the BZ solute, $BZH^+\text{-}(H_2O)_4$ (Fig. S6 in the supplementary material).[45] The origin transition at 29 462 cm^{-1} is shifted to the blue by 910 cm^{-1} from the value obtained for cw3-1.

IV. FURTHER DISCUSSION

The IRPD spectra and the calculations provide a clear picture about the structure of the $[BZ\text{-}(H_2O)_n]H^+$ complexes.

In particular, the protonation site in the ground and $\pi\pi^*$ excited states are fully consistent with the PA values listed in Table I (Fig. S7 in the supplementary material).[45] One has to bare in mind that the PA values can only provide a rough guide for the preferred protonation site because of the importance of solvation energy which may switch the protonation site (as in [benzene-H_2O]H^+),[35,36,40] and also the fact that the topology of the H_2O solvent network may change upon adding the BZ moiety. Both aspects appear to be minor issues for the [BZ-($H_2O)_n$]H^+ clusters. According to the PA in the S_0 state, the [BZ-($H_2O)_n$]H^+ complexes have a BZH^+-($H_2O)_n$ geometry for $n \leq 2$ and a BZ-($H_2O)_n H^+$ structure for $n \geq 3$, i.e. the critical value for (barrierless) ground-state proton transfer to the solvent occurs at the critical hydration size $n_c = 3$. In the S_1 ($\pi\pi^*$) excited state, the PA of BZ is so high, that all [BZ-($H_2O)_n$]H^+ clusters have the BZH^+-($H_2O)_n$ structure for $n \leq 4$. It is unclear, whether the increase in the PA of ($H_2O)_n$ clusters with n will eventually promote proton transfer from BZH^+ to the solvent also in the $\pi\pi^*$ state in the limit $n \to \infty$ (Fig. S7 in the supplementary material).[45] The monotonic shift of the proton from BZ to ($H_2O)_n$ is nicely visible in the calculated bond lengths of the asymmetric $O\cdots H\cdots O$ bridge between both moieties in [BZ-($H_2O)_n$]H^+ (Fig. S8 in the supplementary material).[45] In the S_0 state, the intramolecular O–H bond of BZH^+ is elongated for $n \leq 2$ and transforms into an intermolecular bond after the proton transfer ($n_c = 3$), which is further elongated as n increases. At the same time, the second bond of the $O\cdots H\cdots O$ proton bridge shows the opposite trend. In the S_1 state, the same trend is observed with the exception of the lack of proton transfer in the studied size range. The calculations indicate the $O\cdots H\cdots O$ bridge is so short and strong that the proton can transfer without any significant barrier. Inspection of the IRPD spectra in Fig. 4 reveals that the free O–H stretch frequencies of the terminal and other H_2O ligands (A-C) shift to the blue as n increases. This trend is actually independent of the exact position of the proton and consistent with increasing delocalization of the excess proton, which destabilizes the H-bonds of the solvent network as n increases. Significantly, no free OH band of BZH^+ is observed in any of the spectra, demonstrating the H-bonded solvent cluster binds to the OH proton of BZH^+.

Figure 14 shows the calculated adiabatic energies E_{ad} for the $\pi\pi^*$ transitions of [BZ-($H_2O)_n$]H^+ as a function of the number of solvent molecules for the isomers cis-BZH^+, cw1-1, cw2-1, cw3-1, and cw4-2 (Table IV). In general, the calculated energies are in excellent agreement with available experimental data, suggesting that the ri-CC2/aug-cc-pVDZ level reliably describes the electronic structure in these clusters. As n increases, E_{ad} increases roughly linearly with n and converges toward the value of neutral BZ. This result is expected for larger cluster structures, in which BZ is located on the surface of BZ-($H_2O)_n H^+$ with the charge increasingly delocalized over the solvent cluster as n increases. The IR spectra are consistent with a proton transfer to the solvent for $n \geq 3$ in the S_0 state, in line with the calculations and the PA values listed in Table I. However, due to the much higher PA of BZ in the $\pi\pi^*$ state, cluster structures of [cis-BZ-($H_2O)_n$]H^+ are expected to have the cis-BZH^+-($H_2O)_n$ form in the size range investigated (Fig. S7 in the supplementary material).[45] This
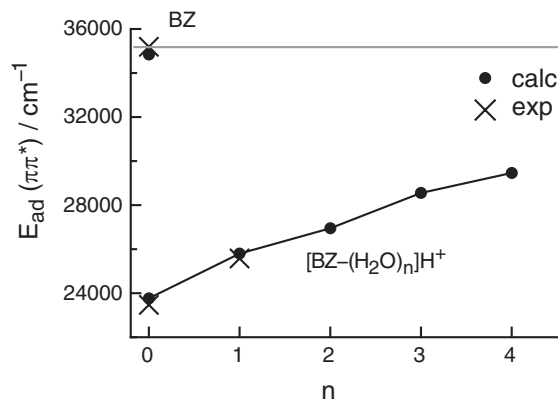

FIG. 14. Calculated and experimental adiabatic energies for the $\pi\pi^*$ transitions of [BZ-($H_2O)_n$]H^+ and BZ (Table IV).

means that for BZ-($H_2O)_n H^+$ with $n \geq 3$, electronic $\pi\pi^*$ excitation should result in a proton transfer from the solvent to the BZ solute (Fig. S6 in the supplementary material).[45] The prediction of $E_{ad} = 26\,948$ cm^{-1} and $E_{vert} = 30\,725$ cm^{-1} for the $\pi\pi^*$ transition of cis-BZH^+-($H_2O)_2$ (Table IV and Fig. 14) explains its absence the electronic spectrum of [BZ-($H_2O)_2$]H^+ measured in the 23 000–27 400 cm^{-1} range.

V. CONCLUDING REMARKS

Vibrational and electronic spectra of protonated microhydrates of benzaldehyde, [BZ-($H_2O)_n$]H^+, recorded by resonance photofragmentation spectroscopy are analyzed using quantum chemical calculations in order to determine the protonation site and solvent structure in the ground and $\pi\pi^*$ excited electronic states. All clusters have structures in which a H-bonded solvent network is attached to BZ(H)$^+$, which binds to the surface of the cluster. In the ground state, the excess proton is attached to BZ for $n \leq 2$ and is transferred to the ($H_2O)_n$ solvent cluster for microhydration sizes larger than $n_c = 3$. In the $\pi\pi^*$ state, the proton remains with BZ in the size range investigated ($n \leq 4$). All observations are in line with the proton affinities for ($H_2O)_n$ and BZ in the ground and $\pi\pi^*$ state, indicating that effects of solvation energies on the location of the proton in these clusters play only a minor role. For clusters with $n \geq 3$, the proton is transferred from the ($H_2O)_n$ solvent to the BZ solute moiety upon $\pi\pi^*$ excitation. The dynamics of this interesting process may be probed in the future by time-resolved spectroscopy. The electronic spectra of [BZ-($H_2O)_n$]H^+ show roughly linear blue shifts as a function of microhydration and converge toward the value of neutral BZ. This trend is relatively independent of the position of the proton in the ground and $\pi\pi^*$ excited states and merely reflect the increasing proton affinity of the ($H_2O)_n$ clusters with size, which shifts the excess proton in both states from BZH^+ to the solvent so that the charge on the aromatic molecule is more and more reduced. The highly interesting behaviour of proton transfer in the ground state as a function of microhydration and proton back transfer upon $\pi\pi^*$ excitation is related to the low proton affinity of BZ in the ground state and high proton affinity in the excited state. Usually, for large microhydrated biomolecules such as peptides with up to

50 H_2O ligands, such effects are not observed,[6] as the ground state proton affinities are typically much larger than those of $(H_2O)_n$ clusters. Moreover, the proton is mostly attached to amino groups far away from the aromatic chromophore(s) so that electronic excitation has essentially no impact on the proton affinity. In general, the IR spectra of $[BZ\text{-}(H_2O)_n]H^+$ converge to those of $(H_2O)_{n+1}H^+$ for large n, indicating that BZ is preferentially solvated on the surface of a protonated water cluster.[44]

ACKNOWLEDGMENTS

[1] V. A. Koptyug, Top. Curr. Chem. **122**, 1 (1984); M. B. Smith and J. March, *Advanced Organic Chemistry: Reactions, Mechanisms, and Structure*, 5th ed. (Wiley, New York, 2001); G. A. Olah, Angew. Chem., Int. Ed. **34**, 1393 (1995); K. H. Homann, *ibid.* **37**, 2434 (1998).

[2] A. G. G. M. Tielens, Annu. Rev. Astron. Astrophys. **46**, 289 (2008); T. Snow, L. V. Page, Y. Keheyan *et al.*, Nature (London) **391**, 259 (1998); U. J. Lorenz, N. Solca, J. Lemaire *et al.*, Angew. Chem., Int. Ed. **46**, 6714 (2007); H. Knorke, J. Langer, J. Oomens *et al.*, Astrophys. J. Lett. **706**, L66 (2009); O. Dopfer, in *PAHs and the Universe: A Symposium to Celebrate the 25th Anniversary of the PAH Hypothesis*, edited by A. G. G. M. Tielens and C. Joblin (EAS Publication Series, 2011), Vol. 46, p. 103.

[3] A. M. Ricks, G. E. Douberly, and M. A. Duncan, Astrophys. J. **702**, 301 (2009); I. Alata, C. Dedonder, M. Broquier *et al.*, J. Am. Chem. Soc. **132**, 17483 (2010).

[4] I. Alata, R. Omidyan, M. Broquier *et al.*, Phys. Chem. Chem. Phys. **12**, 14456 (2010).

[5] T. R. Rizzo, J. A. Stearns, and O. V. Boyarkin, Int. Rev. Phys. Chem. **28**, 481 (2009); A. Svendsen, U. J. Lorenz, O. V. Boyarkin *et al.*, Rev. Sci. Instrum. **81**, 073107 (2010); C. M. Leavitt, A. B. Wolk, J. A. Fournier *et al.*, J. Phys. Chem. Lett. **3**, 1099 (2012); J. G. Redwine, Z. A. Davis, N. L. Burke *et al.*, Int. J. Mass Spectrom. **348**, 9 (2013); A. Fujihara, H. Matsumoto, Y. Shibata *et al.*, J. Phys. Chem. A **112**, 1457 (2008); G. E. Douberly, A. M. Ricks, P. V. R. Schleyer *et al.*, *ibid.* **112**, 4869 (2008); F. X. Hardy, O. Gause, C. A. Rice *et al.*, Astrophys. J. Lett. **778**, L30 (2013); O. Krechkivska, Y. Liu, K. L. K. Lee *et al.*, J. Phys. Chem. Lett. **4**, 3728 (2013); C. Marian, D. Nolting, and R. Weinkauf, Phys. Chem. Chem. Phys. **7**, 3306 (2005); I. Alata, J. Bert, M. Broquier *et al.*, J. Phys. Chem. A **117**, 4420 (2013); I. Alata, R. Omidyan, M. Broquier *et al.*, Chem. Phys. **399**, 224 (2012); I. Alata, M. Broquier, C. Dedonder *et al.*, *ibid.* **393**, 25 (2012); N. Solcà and O. Dopfer, Chem. Phys. Lett. **342**, 191 (2001); Angew. Chem., Int. Ed. **41**, 3628 (2002); J. Am. Chem. Soc. **126**, 1716 (2004); Angew. Chem., Int. Ed. **42**, 1537 (2003); F. M. Pasker, N. Solcà, and O. Dopfer, J. Phys. Chem. A **110**, 12793 (2006); A. Patzer, M. Schütz, C. Jouvet *et al.*, J. Phys. Chem. A **117**, 9785 (2013).

[6] N. S. Nagornova, T. R. Rizzo, and O. V. Boyarkin, Science **336**, 320 (2012).

[7] I. Alata, R. Omidyan, C. Dedonder-Lardeux *et al.*, Phys. Chem. Chem. Phys. **11**, 11479 (2009).

[8] I. Alata, M. Broquier, C. Dedonder-Lardeux *et al.*, J. Chem. Phys. **134**, 074307 (2011).

[9] N. Solcà and O. Dopfer, J. Am. Chem. Soc. **125**, 1421 (2003).

[10] A. Patzer, M. Zimmermann, I. Alata *et al.*, J. Phys. Chem. A **114**, 12600 (2010).

[11] S. Chakraborty, A. Patzer, and O. Dopfer, J. Chem. Phys. **133**, 044307 (2010).

[12] M. Bahou, Y. J. Wu, and Y. P. Lee, J. Chem. Phys. **136**, 154304 (2012); Phys. Chem. Chem. Phys. **15**, 1907 (2013); J. Phys. Chem. Lett. **4**, 1989 (2013); I. Garkusha, J. Fulara, A. Nagy *et al.*, J. Am. Chem. Soc. **132**, 14979 (2010); I. Garkusha, J. Fulara, and J. P. Maier, J. Mol. Struct. **1025**, 147 (2012); I. Garkusha, A. Nagy, J. Fulara, *et al.*, J. Phys. Chem. A **117**, 351 (2013).

[13] B. Brutschy, Chem. Rev. **92**, 1567 (1992).

[14] O. Dopfer, Z. Phys. Chem. **219**, 125 (2005).

[15] K. Kleinermanns, C. Janzen, D. Spangenberg *et al.*, J. Phys. Chem. A **103**, 5232 (1999).

[16] M. Miyazaki, A. Fujii, T. Ebata *et al.*, Chem. Phys. Lett. **399**, 412 (2004).

[17] M. Miyazaki, A. Fujii, T. Ebata *et al.*, Phys. Chem. Chem. Phys. **5**, 1137 (2003).

[18] N. Solcà and O. Dopfer, J. Phys. Chem. A **107**, 4046 (2003).

[19] S. R. Mercier, O. V. Boyarkin, A. Kamariotis *et al.*, J. Am. Chem. Soc. **128**, 16938 (2006).

[20] T. M. Chang, J. S. Prell, E. R. Warrick *et al.*, J. Am. Chem. Soc. **134**, 15805 (2012).

[21] G. A. Olah, G. Rasul, C. York *et al.*, J. Am. Chem. Soc. **117**, 11211 (1995).

[22] B. Chiavarino, M. E. Crestoni, S. Fornarini *et al.*, J. Phys. Chem. A **110**, 9352 (2006).

[23] B. S. Freiser and J. L. Beauchamp, J. Am. Chem. Soc. **99**, 3214 (1977).

[24] C. J. Cassady, B. S. Freiser, and D. H. Russell, Org. Mass Spectrom. **18**, 378 (1983).

[25] O. Dopfer, Int. Rev. Phys. Chem. **22**, 437 (2003); M. Fujii and O. Dopfer, *ibid.* **31**, 131 (2012).

[26] A. Patzer, S. Chakraborty, and O. Dopfer, Phys. Chem. Chem. Phys. **12**, 15704 (2010).

[27] C. Camy-Peyret, J. M. Flaud, G. Guelachvili *et al.*, Mol. Phys. **26**, 825 (1973).

[28] M. J. Frisch, G. W. Trucks, H. B. Schlegel *et al.*, Gaussian 09, Revision A.02, Gaussian, Inc., Wallingford, CT, 2009.

[29] P. J. Linstrom and W. G. Mallard, *NIST Chemistry WebBook* (NIST Standards and Technology, Gaithersburg MD, 2014), see http://webbook.nist.gov.

[30] R. Ahlrichs, M. Bär, M. Häser *et al.*, Chem. Phys. Lett. **162**, 165 (1989).

[31] C. M. Western, PGOPHER, University of Bristol, Bristol, U.K., 2010, see http://pgopher.chm.bris.ac.uk.

[32] N. Solcà and O. Dopfer, Chem. Phys. Lett. **347**, 59 (2001).

[33] M. Miyazaki, A. Fujii, T. Ebata *et al.*, Chem. Phys. Lett. **349**, 431 (2001).

[34] U. Lorenz, N. Solcà, and O. Dopfer, Chem. Phys. Lett. **406**, 321 (2005); S. Chakraborty, A. Patzer, A. Lagutschenkov *et al.*, *ibid.* **485**, 49 (2010); Int. J. Mass Spectrom. **297**, 85 (2010).

[35] E. S. Kryachko and M. T. Nguyen, J. Phys. Chem. A **105**, 153 (2001).

[36] T. C. Cheng, B. Bandyopadhyay, J. D. Mosley *et al.*, J. Am. Chem. Soc. **134**, 13046 (2012).

[37] C. Unterberg, A. Jansen, and M. Gerhards, J. Chem. Phys. **113**, 7945 (2000); K. Tanabe, M. Miyazaki, M. Schmies *et al.*, Angew. Chem., Int. Ed. **51**, 6604 (2012).

[38] H. Abe, S. Kamei, N. Mikami *et al.*, Chem. Phys. Lett. **109**, 217 (1984).

[39] C. R. Silva and J. P. Reilly, J. Phys. Chem. **100**, 17111 (1996).

[40] N. Solcà and O. Dopfer, Chem. Eur. J. **9**, 3154 (2003).

[41] D. J. Goebbert and P. G. Wenthold, Eur. J. Mass Spectrom. **10**, 837 (2004).

[42] E. P. L. Hunter and S. G. Lias, J. Phys. Chem. Ref. Data **27**, 413 (1998).

[43] G. Herzberg, *Molecular Spectra and Molecular Structure. II. Infrared and Raman Spectra of Polyatomic Molecules* (Krieger Publishing Company, Malabar, Florida, 1991).

[44] A. Fujii and K. Mizuse, Int. Rev. Phys. Chem. **32**, 266 (2013).

[45] See supplementary material at http://dx.doi.org/10.1063/1.4869341 for (1) structures of cw1-x and tw1-x isomers, (2) NBO charges of $[cis\text{-}BZ\text{-}(H_2O)_n]H^+$ with $n \leq 4$, (3) IR spectrum of $H_3O^+\text{-}BZ(\pi)$, (4) molecular orbitals, (5) and (6) structures of $[cis\text{-}BZ\text{-}(H_2O)_n]H^+$ with $n \leq 4$ in S_0 and S_1, (7) PA of $(H_2O)_n$ and BZ in S_0 and $\pi\pi^*$ state, (8) bond distances in the $O \cdots H \cdots O$ proton bridge in $[cis\text{-}BZ\text{-}(H_2O)_n]H^+$.